Dalton Transactions

Accepted Manuscript

This article can be cited before page numbers have been issued, to do this please use: A. K. Singh, R. N. N. Pradhan, S. Chakraborty, A. Ghosh, P. Bharti and J. Kumar, *Dalton Trans.*, 2019, DOI: 10.1039/C9DT00747D.

This is an Accepted Manuscript, which has been through the Royal Society of Chemistry peer review process and has been accepted for publication.

Accepted Manuscripts are published online shortly after acceptance, before technical editing, formatting and proof reading. Using this free service, authors can make their results available to the community, in citable form, before we publish the edited article. We will replace this Accepted Manuscript with the edited and formatted Advance Article as soon as it is available.

You can find more information about Accepted Manuscripts in the author guidelines.

Please note that technical editing may introduce minor changes to the text and/or graphics, which may alter content. The journal's standard Terms & Conditions and the ethical guidelines, outlined in our author and reviewer resource centre, still apply. In no event shall the Royal Society of Chemistry be held responsible for any errors or omissions in this Accepted Manuscript or any consequences arising from the use of any information it contains.

ROYAL SOCIETY OF CHEMISTRY

rsc.li/dalton

View Article Online
DOI: 10.1039/C9DT00747D

Seven Coordinate Co(II) and Six Coordinate Ni(II) Complexes of Aromatic Macrocyclic Triamide Ligand as ParaCEST Agents for MRI†

Rabindra N. Pradhan,[a] Subhayan Chakraborty,[b] Pratibha Bharti,[c] Janesh Kumar,[c] Arindam Ghosh,*[b] and Akhilesh K. Singh*[a]

[a]School of Basic Sciences, Indian Institute of Technology Bhubaneswar, Bhubaneswar, 752050 (India), E-mail: aksingh@iitbbs.ac.in
[b]School of Chemical Sciences, National Institute of Science Education and Research Bhubaneswar, 752050 (India), E-mail: aringh@niser.ac.in
[c]National Centre for Cell Science, NCCS Complex, Pune University Campus, Ganeshkhind, Pune-411 007 (India)

†Electronic supplementary information (ESI) available: 1H NMR, electrospray ionization (ESI)-MS, magnetic susceptibility data, Cyclic voltammogram, MTT assay, Omega plot, CCDC 1884844 and 1884845.

We are reporting Co(II) and Ni(II) complexes of a pyridine containing aromatic macrocyclic triamide ligand, 3,6,9,15-tetraazabicyclo(9.3.1)pentadeca-1(15),11,13-triene-3,6,9-triacetamide (**TPTA**) as paramagnetic chemical exchange saturation transfer (paraCEST) MRI contrast agent. The synthesis and characterization of **TPTA** and its complexes are reported. The solution chemistry and solid-state structure of Co(II) and Ni(II) complexes are studied. Crystallographic data show that [Co(**TPTA**)]·Cl_2·$2H_2O$ complex (seven-coordinate, all four N atoms of ring and three amide O atoms) has distorted pentagonal bipyramidal geometry however [Ni(**TPTA**)Cl]·Cl·$0.25H_2O$ complex (six-coordinate, all four N atoms of the ring, one amide O and one chloride ion) adopts distorted octahedral geometry. Notably the two pendent amide arms are not coordinated in [Ni(**TPTA**)Cl]$^{+1}$ complex and one chloride ion fulfils its sixth coordination. The CEST effect of [Co(**TPTA**)]$^{+2}$ and [Ni(**TPTA**)Cl]$^{+1}$ amide protons are observed at 57 ppm and 78 ppm downfield of the bulk water proton respectively in buffer solution containing 20 mM N-(2-hydroxyethyl)piperazine-N'-ethanesulfonic acid and 100 mM NaCl at pH 7.4 at 37 ºC on a 9.4 T NMR spectrometer. The effect of CEST intensity and exchange rate constant with variation of pH of the solution were studied. The CEST effect and exchange rate constant for amide protons of [Co(**TPTA**)]$^{+2}$ complex have been monitored in HEPES buffer, fetal bovine serum (FBS), rabbit serum and 4% agarose gel (w/w). The stability of the [Co(**TPTA**)]$^{+2}$ complex in aqueous solution towards oxidation was verified by using cyclic voltammetry measurement. The stability of [Co(**TPTA**)]$^{+2}$ has further been monitored in presence of biologically relevant ions including HPO_4^{-2}, CO_3^{-2}, Zn^{+2} and under acidic conditions.

Introduction

Magnetic resonance imaging (MRI) is one of the most significant accepted non-invasive diagnostic imaging tool for in vivo application. The main advantage of MRI is lack of non-ionizing radiation

View Article Online
DOI: 10.1039/C9DT00747D

and excellent depth penetration offering high resolution images of soft tissues.[1-5] The majority of the clinically approved contract agents are based on difference in the proton density and T1 and T2 relaxation rates of water protons present in the tissue and organs.[6-9] So far the conventional contrast agents are lanthanide based complexes, typically Gd(III) complexes, that shorten the longitudinal (T1) relaxation times of water protons and provide high resolution images.[10] The first generation of contrast agents have limited physical properties and their preinjection and postinjection scans are time-consuming, although these are widely used for clinical medicine.[11, 12] Over the past decades the new generation of MRI contrast agents was devolved which was operated by chemical exchange saturation transfer (CEST) techniques, able to provide spatial resolution and metabolic informations.[13-16] In order to observe CEST effect the chemical shift difference between bulk water protons and exchangeable protons ($\Delta\omega$) must be equal or higher than the rate of chemical exchange (k_{ex}) between two pools.[11, 12, 17]

For last few years, it has been observed that divalent transition metal ion complexes of macrocyclic and acyclic ligands as paramagnetic chemical exchange saturation transfer (paraCEST) contrast agents have been of great interest in magnetic resonance imaging (MRI).[18-24] This type of contrast agents provide potential advantages over lanthanide, Ln(III) contrast agents. The discrete coordination chemistry of first row transition metal ions motivates to develop new type of paraCEST contrast agents which provide opportunities for application in broad area of MRI imaging. Co(II), Fe(II), and Ni(II) complexes are mostly used as effective paraCEST contrast agents among all transition metal ion complexes.[18-20, 24] The paramagnetic centre interacts with ligand protons not only through bond but also through space to produce sharp and highly shifted ^{1}H proton resonance on the NMR time scale.[25-27] The paramagnetic metal complexes that show paraCEST properties must be associated with exchangeable protons (-NH, -OH, or bound water) that exchange with the bulk water.[28-33] To get contrast in presence of paraCEST agents, selective irradiation of radiofrequency pulse is applied to a pool of exchangeable protons which are in slow to intermediate exchange with bulk water protons which causes decrease in the magnetization of these exchanging protons. This phenomena leads to decrease in the water proton signal.[11, 17, 34, 35]

In order to produce thermodynamically stable and kinetically inert metal-based paraCEST probe at physiological pH and temperature, typically the metal complexes of ligands containing N and O donors are used. The multidentate ligands form rigid six-[22-24, 36], seven-[20, 21] and eight-coordinate[19, 21] complexes with Fe(II), Co(II), or Ni(II) making it possible to produce limited broadening and large proton shift in ^{1}H spectra.[25, 26] The ligands must contain hetero atom donor groups like amides, alcohol, pyridines, imidazole and pyrazoles with exchangeable protons that chemically exchange with water. Morrow and other research groups have reported several macrocyclic ligands with different pendent arms (1,4,7-triazacyclononane (tacn)[21, 24], 1,4,7,10-tetraazacyclododecane (cyclen),[19, 37] 1,4,8,11-tetraazacyclotetradecane (cyclam),[22] 1,4,10-trioxa-7,13-diazacyclopentadecane[18, 20]) derivatives, whereas Harris and co-workers have reported amide-appended acyclic ligands (2-hydroxy-5-nitro-1,3-phenylene)bis(methylene)[23, 38] whose transition metal complexes provide stable and efficient paraCEST contrast agents.

In the present work, we introduce for the first time a novel pyridine containing macrocyclic backbone 3,6,9,15-tetraazabicyclo(9.3.1)pentadeca-1(15),11,13-triene-3,6,9-triacetamide ligand **(TPTA,** Chart 1**)** for transition metal paraCEST contrast agent with amide donor groups that produce a CEST effect through exchange. Herein, we report the synthesis and characterisation of

View Article Online
DOI: 10.1039/C9DT00747D

the ligand and its corresponding metal complexes [Co(**TPTA**)]·Cl_2·$2H_2O$ and [Ni(**TPTA**)Cl]·Cl·$0.25H_2O$. Effective magnetic moment in solution state and CEST properties of the both structurally characterized complexes were investigated. The dissociation of $[Co(\mathbf{TPTA})]^{+2}$ complex is studied in acidic condition as well as in presence of biologically relevant ions such as carbonate, Zn(II) and phosphate. The redox behaviour of $[Co(\mathbf{TPTA})]^{+2}$ complex was investigated in aqueous solution. The exchangeable carboxamide protons of $[Co(\mathbf{TPTA})]^{+2}$ complex show noticeable change in CEST properties with variation of pH. The maximum CEST intensity of the $[Co(\mathbf{TPTA})]^{+2}$ complex is observed at pH 7.8. Interestingly the $[Co(\mathbf{TPTA})]^{+2}$ complex retains its CEST activity in different media including rabbit serum, fetal bovine serum (FBS) and 4% agarose gel (w/w), which makes it suitable for potential application in living systems. The biocompatibility has been evaluated using tissue culture in HEK cell, which shows no toxicity up to 10 mM concentration.

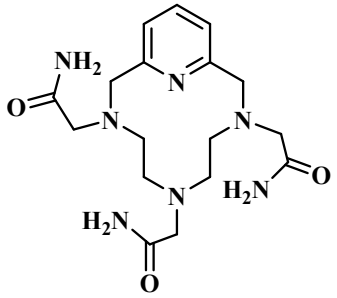

TPTA

Chart 1 Structure of ligand **TPTA**

Results and discussion

Synthesis and crystal structure

The macrocylic 3,6,9,15-tetraazabicyclo[9.3.1]pentadeca-1(15),11,13-triene (**3**) was prepared by slight modification of the previously reported procedure[39] which involved the synthesis of 3,6,9-tris(p-tolylsulfonyl)-3,6,9,15-tetraazabicyclo[9.3.1]pentadeca1(15),11,13-triene (**2**) and subsequent deprotection of the tosyl groups by sulfuric acid. Then alkylation of the three secondary amine groups of **3** with 2-bromoacetamide yielded the ligand **TPTA**. The corresponding metal complexes were isolated by addition of stoichiometric amounts (1:1) of the ligand and the chloride salts of Co(II), and Ni(II) in methanol (see Experimental Section for details). To explore the coordination environment around central metal ions of these complexes, their structures were characterized by single crystal X-ray diffraction.

Slow evaporation of diethyl ether vapour into concentrated solution of [Co(**TPTA**)]·Cl_2·$2H_2O$ in MeOH afforded pink coloured block like crystals and slow evaporation of [Ni(**TPTA**)Cl]$_2$·Cl_2·$0.5H_2O$ in a mixture of DMF and MeOH yielded plate like bluish crystals. X-ray diffraction data indicated that both complexes $[Co(\mathbf{TPTA})]^{+2}$ and $[Ni(\mathbf{TPTA})Cl]^{+2}$ adopted triclinic unit cell with a space group of P-1 (Table 2 in Experimental section). In $[Co(\mathbf{TPTA})]^{+2}$ all nitrogen atoms (N1, N2, N4, N6) of macrocyclic backbone and oxygen atoms (O1, O2, O3) of the pendent carboxamide groups formed a seven coordinate complex. The coordination polyhedra

View Article Online
DOI: 10.1039/C9DT00747D

around the metal ion (Co(II)) can be best described as a distorted pentagonal bipyramidal geometry (Fig. 1). Three amine-N atoms (N2, N4 and N6) of macrocyclic ring and two amide-O (O1 and O3) of the pendent arms form the pentagonal base, and the pyridine-N atom (N1) of the macrocyclic backbone and the amide-O (O2) of remaining pendent arm occupy the axial positions (Fig. 1). [Co(**TPTA**)]$^{+2}$ complex has two types (axial and equatorial) of metal-nitrogen and metal-oxygen bonds. The axial Cobalt-nitrogen (pyridine) (Co1-N1) bond is shorter than other Cobalt-nitrogen bonds in the macrocyclic backbone. The average Co1-O and Co1-N bond distances of [Co(**TPTA**)]$^{+2}$ are 2.185(5) Å and 2.227(5) Å, respectively. The axial bond angle of N1-Co1-O2 is 172.9(2), confirms that both N1 and O2 are in axial position of the pentagonal bipyramidal structure (Fig. 1 and Table S2, ESI†). The overall charge balance for Co(II) is confirmed by the presence of two chloride anions.

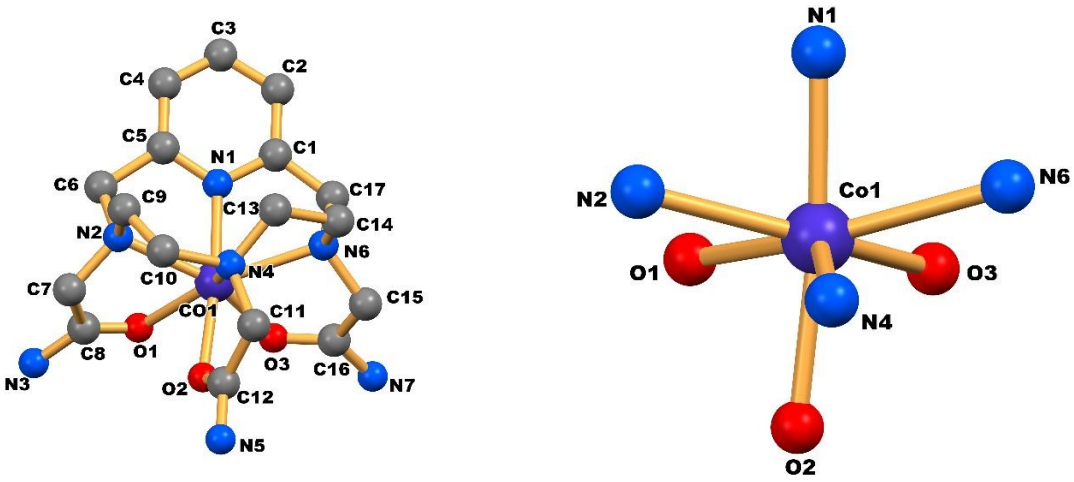

Fig. 1 X-ray crystal structural of the [Co(**TPTA**)]·Cl_2·$2H_2O$ complex. For clarity, the solvent, hydrogen and counter ions were omitted in the structure.

The [Ni(**TPTA**)Cl]$_2$·Cl_2·$0.5H_2O$ complex has six coordinated metal centre. The Ni(II) ion is bound to four nitrogen atoms of macrocyclic ring (N1, N2, N4, N6), one amide oxygen (O1) of pendent arm and one chloride ion to give a distorted octahedral geometry (Fig. 2). The remaining two pendent arms of the ligand are dangling and not coordinated to the metal centre. The amide-O (O1) and the pyridine-N (N1) are oriented in trans position to each other to give a distorted octahedral geometry. This distortion can be attributed to Jahn-Teller effect. The axial bonds with bond length of 2.015(3) and 2.083(3) Å for Ni1-N1 and Ni1-O1 respectively are shorter than other bonds (see in the SI Table S2). The average bond length of other three nitrogen atoms (N2, N4, N6) is 2.191 (3) Å (see in the SI Table S2) and the bond length of Ni1-Cl1 is 2.336 (3), which is little longer than other bonds. The important bond lengths and bond angles are given in the Supporting Information (Table S2).

View Article Online
DOI: 10.1039/C9DT00747D

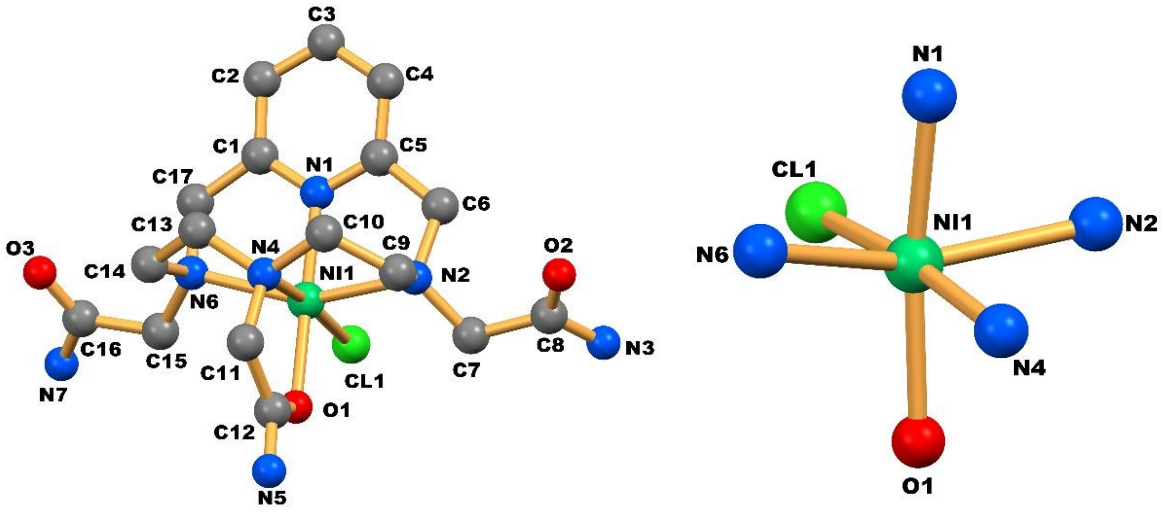

Fig. 2 X-ray crystal structural of the $[Ni(\mathbf{TPTA})]_2{\cdot}Cl_2{\cdot}0.5H_2O$ complex. For clarity, the solvent, hydrogen and counter ions were omitted in the structure.

Solution magnetic properties

In order to confirm the dissociation of chloride ion in [Ni(**TPTA**)Cl]Cl complex, the complex (1:1 electrolyte in solid state) was dissolved in water and its molar conductance was measured. Most likely the bound chloride ion is dissociated and it is exchanged with water because the obtained molar conductance value (192 $ohm^{-1}cm^2mol^{-1}$) lie in the range of 1:2 electrolyte (145-273 $ohm^{-1}cm^2mol^{-1}$).[40] In aqueous buffer solutions the effective magnetic moment of $[Co(\mathbf{TPTA})]^{+2}$ and $[Ni(\mathbf{TPTA})Cl]^{+1}$ complexes with variation of pH 6.5-8.4 were obtained at 37 ºC using Evans method (see experimental section). The resulting plot of $\chi_M T$ versus pH (see Fig. S23 and S24, ESI†) ensure that the variation of $\chi_M T$ values is insignificant with variation of pH. The average effective magnetic moments of $[Co(\mathbf{TPTA})]^{+2}$ and $[Ni(\mathbf{TPTA})Cl]^{+1}$ are obtained 4.07 ± 0.10 and 3.05 ± 0.02 μ_B respectively. These values are in the expected range for structurally reported similar high spin Co(II) and Ni(II) complexes at physiological pH at 37 °C in aqueous solution.[26, 27] The effective magnetic moment of $[Co(\mathbf{TPTA})]^{+2}$ complex was measured in biological media like rabbit serum and FBS at pH 7.4 were found to be 4.16 and 4.22 μ_B respectively.

NMR spectroscopy

In order to investigate the solution properties of $[Co(\mathbf{TPTA})]^{+2}$ and $[Ni(\mathbf{TPTA})Cl]^{+1}$ complexes, ^1H NMR spectra were collected in DMSO, D_2O and buffer solutions. In D_2O, $[Co(\mathbf{TPTA})]^{+2}$ exhibits total 9 proton resonances ranging from 0 to 170 ppm at 25 °C (**Fig. 3**), with two exchangeable carboxamide protons at 63 and 68 ppm, identified by the decrease in intensity of these peaks observed in the analogous spectrum after addition of D_2O in DMSO-d_6 (**Fig.** S16, ESI†). Out of these 9 proton resonances, one proton resonance is found within diamagnetic regions (Fig. 3). The 8 paramagnetic resonances have equivalent integrated intensities, while the resonance within diamagnetic regions has half integrated intensity. The ^1H-^1H-COSY spectrum allowed us to identify the resonances at 10.31 and 42.05 in D_2O as the aromatic protons of the $[Co(\mathbf{TPTA})]^{+2}$ (Fig. S19, ESI†), while the other 7 paramagnetic proton resonances correspond to CH_2 peaks of the complex. In the ^1H NMR spectra recorded at variable temperatures ranging from 25 °C to 60

View Article Online
DOI: 10.1039/C9DT00747D

°C, the peak widths of the resonances changed very little upon increase in temperature (Fig. S20, ESI†). This suggests that the dynamic processes do not have much effect on the line broadening over this temperature range. The ^{1}H NMR resonances of two paramagnetic CH_2 peaks at 167.5 and 107.8 in D_2O are highly-shifted towards upfield with increase in the temperature from 25 °C to 60 °C (Fig. S21, ESI†), similar to the reported Co(II) complex.[40] However, ^{1}H NMR spectra shows significant broadening of the exchangeable protons when pH of the solution is increased in the range of 6.10 to 8.40 for the [Co(**TPTA**)]$^{+2}$ complex, confirming base catalysed proton exchange[23, 37] (Fig. S25, ESI†).

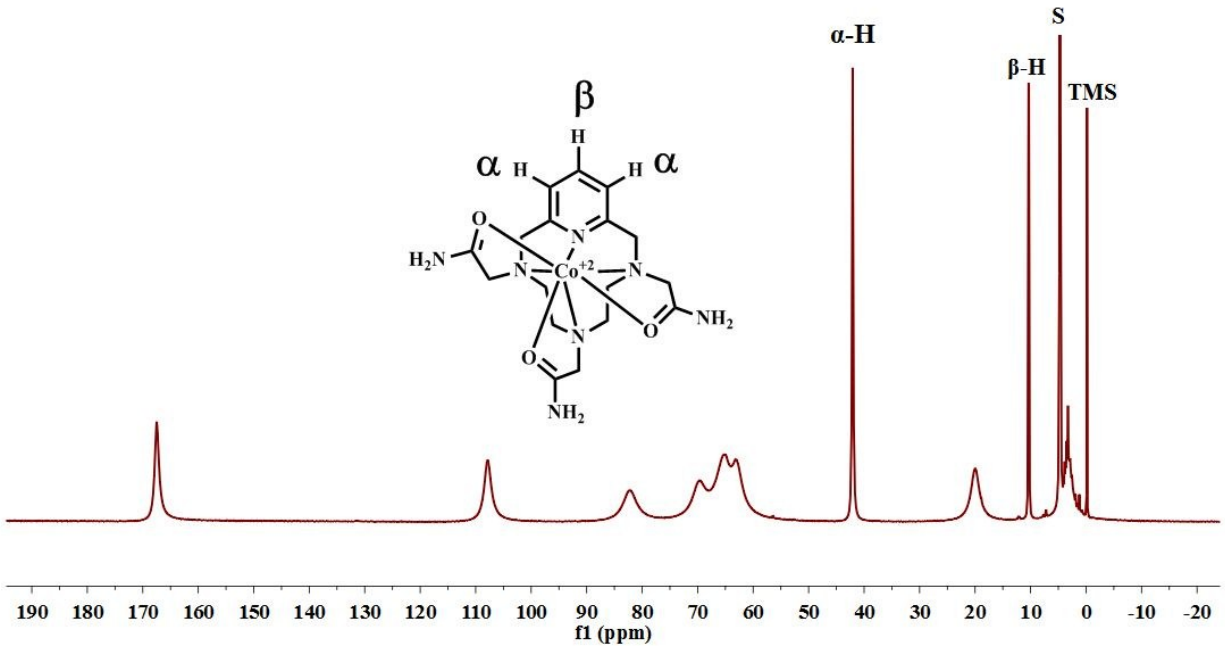

Fig. 3 ^{1}H NMR spectrum of [Co(**TPTA**)]$^{+2}$ in deuterium oxide.

In comparison, the proton NMR spectrum of [Ni(**TPTA**)Cl]$^{+1}$ exhibits 7 paramagnetic proton resonances ranging from 0 to 150 ppm in D_2O (see Fig. S18 ESI†), with exchangeable carboxamide signals at 7, 13 and 78 ppm, confirmed by comparison of the spectra recorded in DMSO-d_6 and after addition of D_2O in DMSO-d_6 (see Fig. S17, ESI†). The resonances of two unbounded exchangeable carboxamide protons are slightly shifted downfield from the diamagnetic region at 7 and 13 ppm which were similar to the reported six coordinated Ni(II) complex.[22] Additionally one highly shifted amide proton resonance at 78 ppm was observed. Like many Ni(II) complexes, the [Ni(**TPTA**)Cl]$^{+1}$ complex shows broad peaks due to its long electronic relaxation time.[42]

Redox properties

To investigate the inertness of the [Co(**TPTA**)]$^{+2}$ complex in solutions towards oxidation, cyclic voltammetry experiment was performed in an aqueous buffer solution at pH 7.4. The [Co(**TPTA**)]$^{+2}$ complex shows an irreversible oxidative response at E(peak) = 792 mV versus NHE which corresponds to Co(III)/Co(II) redox couple (see Fig. S39, ESI). The higher positive

View Article Online
DOI: 10.1039/C9DT00747D

value for the oxidative response suggests the stability of [Co(**TPTA**)]$^{+2}$ complex towards oxidation in aqueous solution.[43]

Dissociation of complex

To determine the dissociation of the [Co(**TPTA**)]$^{+2}$ complex, ^{1}H NMR spectra of the complex in paramagnetic and diamagnetic regions were monitored. Under acidic condition (pD-3.96) the [Co(**TPTA**)]$^{+2}$ complex dissociated by 6% over 72 h at 37 °C (see Fig. S27 and S28, ESI†). In presence of equimolar concentration of competing Zn(II) ions at 37 °C, pD-7.01 for 72 h , [Co(**TPTA**)]$^{+2}$ complex did not show any evidence of metal ion dissociation, as the intensity of proton resonances remain constant as compared to the standard at neutral pH (see Fig. S27 and S30, ESI†). In order to further determine the stability of [Co(**TPTA**)]$^{+2}$ complex in the presence of high concentrations of carbonate and phosphate under physiological condition, 10 mM complex at pD 7.34 was incubated with 100 mM NaCl, 25 mM K_2CO_3, 0.40 mM Na_2HPO_4 at 37 °C and was monitored for 72 h. The ^{1}H spectra were recorded at different time interval revealed that the complex does not dissociate even in the presence of high concentration of anions (see Fig. S27 and S29, ESI†). Notably, the intensity of proton resonances decreased under these conditions which indicates some interaction with the anions, but such interaction did not alter the CEST efficiency (see Fig. S37, ESI†). Taken altogether, the stability of [Co(**TPTA**)]$^{+2}$ complex is very high under physiological conditions which paves the way of its potential application as an MRI contrast agent for in vivo studies. As the two pendent amide arms in [Ni(**TPTA**)Cl]$^{+1}$ are not coordinated to the Ni^{+2} and this complex exhibits very low CEST intensity as compared to [Co(**TPTA**)]$^{+2}$**,** the [Ni(**TPTA**)Cl]$^{+1}$ complex could not be studied in a similar way like the [Co(**TPTA**)]$^{+2}$ complex.

Biological characterizations

To investigate the cytotoxicity in vitro the [Co(**TPTA**)]$^{+2}$ complex was examined using MTT assay on HEK 293 WT cell line. The cells were incubated at different concentration of the complex (1-10 mM) for 24 h at 37 °C. The complex did not show significant toxicity up to the tested concentration of 10 mM (see Fig. S38, ESI†). After 24 hours of treatment with the compound, the cell viability remained unchanged.

CEST properties

In order to investigate the paraCEST properties of [Co(**TPTA**)]$^{+2}$ and [Ni(**TPTA**)Cl]$^{+1}$ complexes, the CEST spectra were collected with 10 mM complexes, 100 mM NaCl, and 20 mM of HEPES buffer at 37 °C. The [Co(**TPTA**)]$^{+2}$ and [Ni(**TPTA**)Cl]$^{+1}$ complexes produced downfield-shifted peak at 57 and 70 ppm respectively verses bulk water (Fig. 4). CEST peak at 57 ppm downfield from bulk water protons for [Co(**TPTA**)]$^{+2}$ complex is attributed to the distinct exchangeable amide (NH) protons at 68 and 63 ppm in DMSO-d_6 (see Fig. S16, ESI†) and the CEST peak at 70 ppm is attributed to the exchangeable amide proton at 78 ppm in DMSO-d_6 (see Fig. S17 ESI†). The CEST signals for the exchangeable NH protons at 7 ppm for [Ni(**TPTA**)Cl]$^{+1}$ complex is concealed by direct saturation of bulk water protons.

View Article Online
DOI: 10.1039/C9DT00747D

Unlike [Co(**TPTA**)]$^{+2}$ in buffer medium, the [Ni(**TPTA**)Cl]$^{+1}$ complex does not show appreciable CEST effect due to the fact that the exchange constant and T_1 relaxivity of the complex is larger than the [Co(**TPTA**)]$^{+2}$ complex.

The CEST effect as expected was found to be very sensitive to the pH level of the solution and the [Co(**TPTA**)]$^{+2}$ complex showed maximum CEST effect at pH 7.8. Fig. 5 compares the z-spectra (top, the exchangeable proton region around 57 ppm and bottom, CEST effect) at pH ranging from 6.8 to 8.3. The CEST intensity increases with increase in the pH in the range of 6.8 to 7.8, consistent with the base catalysed proton exchange of carboxamide protons. The gradual decrease of CEST efficiency at more basic pH is attributed to faster exchange, leading to exchange broadening for amide protons. Similar pH dependence trends were observed for paraCEST contrast agents containing amide pendent for both Ln(III) and transition metal ions.[12, 20, 23, 35] The CEST peak intensity increases almost linearly with pH before it drops marginally beyond pH 7.8. At physiological condition (pH 7.4 and 37 °C) the CEST effect was found to be 30% (Fig. 4). CEST effects were calculated by measuring the difference in normalized water peak intensities from a pair of experiments, one with on resonance saturation of the exchangeable proton (at 57 ppm) and the other by off-resonance saturation at the symmetrically opposite frequency of –57 ppm with respect to bulk water.

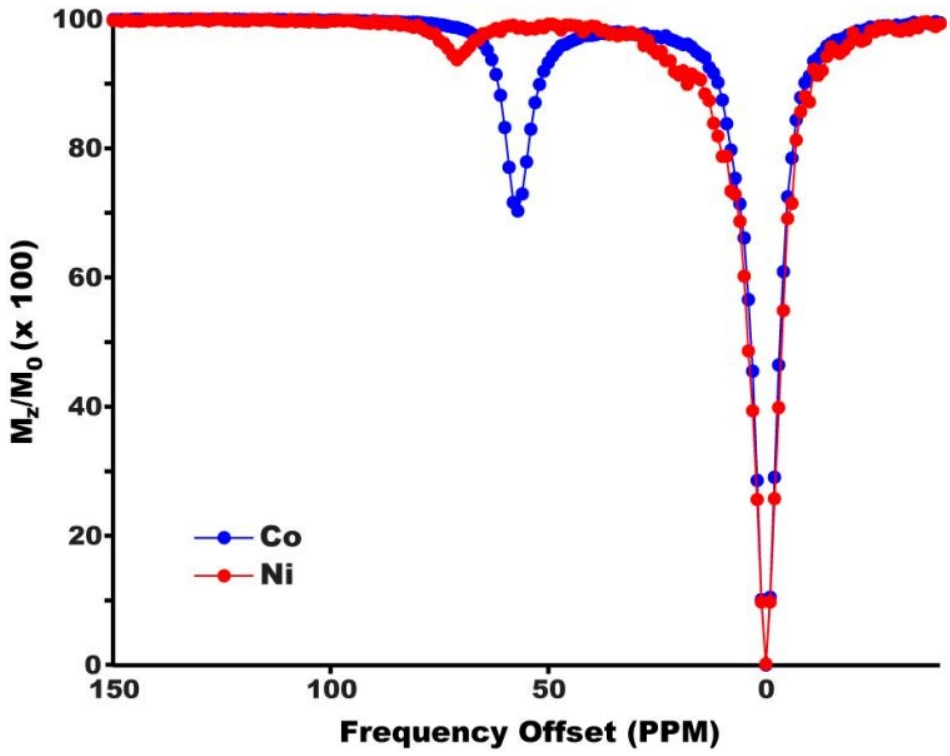

Fig. 4 Overlaid CEST z-spectra of 10 mM complexes [Co**(TPTA)**]$^{+2}$ (blue) and [Ni**(TPTA)**Cl]$^{+1}$ (red)) in 20 mM HEPES buffer and 100 mM NaCl at pH 7.4. RF presaturation pulse was applied for 2 s with B_1 = 25μT at 37 ˚C.

The exchange rate constant k_{ex} of amide (NH) protons of 10 mM [Co(**TPTA**)]$^{+2}$ and 40 mM [Ni**(TPTA)**Cl]$^{+1}$ complexes at 37 ºC in buffer medium containing 20 mM HEPES and 100 mM

View Article Online
DOI: 10.1039/C9DT00747D

NaCl at pH 7.4 were found to be 3691 s^{-1} and 5096 s^{-1} respectively (Fig. S32 and S34, Table S1, ESI†). The exchange rate constant of the Ni(II) complex is nearly three times larger than that of Co(II) complex, so the CEST effect of the Ni(II) complex would be anticipated to decrease. The exchange rate constant of [Co(**TPTA**)]$^{+2}$ increases with increase in the pH in the range of 6.8 to 8.3, consistent with the base catalysed proton exchange of carboxamide protons (Fig. S31, S32 and S33, Table S1, ESI†). At higher pH value of 8.3, rapid proton exchange leads to exchange broadening and a decrease of the CEST peak.[12, 19, 22-24, 36, 44-46] The exchange rate constant at pH 6.8 was found 2379 s^{-1} which is very less as compared to the exchange rate constant 13380 s^{-1} at pH 8.3 (see Fig. S31 and S33, Table S1, ESI†).

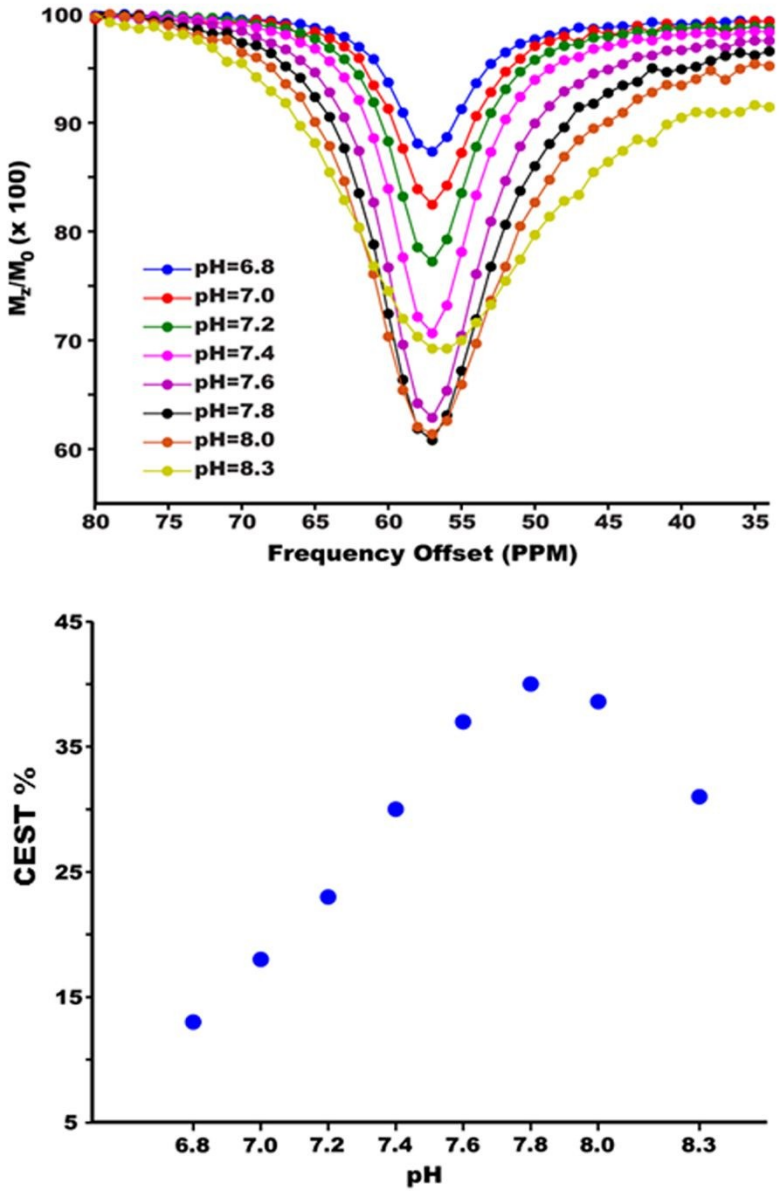

Fig. 5 Dependence of CEST effect on pH. (Top) Overlaid spectra of the exchangeable proton region of 10 mM [Co**(TPTA)**]$^{+2}$ in 20 mM HEPES buffer with pH ranging from 6.8 to 8.3. (Bottom) CEST peak intensity as a function of pH as calculated from the spectra shown in top. All experiments were performed with 2 s presaturation radiofrequency pulse at $B_1 = 25$ μT.

View Article Online
DOI: 10.1039/C9DT00747D

To monitor the efficiency of the [Co(**TPTA**)]$^{+2}$ complex as a CEST agent in biological media, separate 10 mM solutions of the [Co(**TPTA**)]$^{+2}$ complex were prepared in rabbit serum, fetal bovine serum (FBS) and 4% agarose gel at pH 7.4. All spectra were recorded at 37 °C. Fig. 6 shows a comparison of z-spectra of the [Co(**TPTA**)]$^{+2}$ complex in HEPES buffer as well as in the three biological media. The exchange rate constant (k_{ex}) were measured in all three biological media (SI Fig. S35, ESI†) and compared those with aqueous buffer solution (Fig. S32, ESI†). The CEST effect in the physiological condition were found marginally lower in rabbit serum (28%), FBS(25%) and agarose gel (23%) in comparison to the buffered medium (30%). The decrease in CEST effect in rabbit serum by (2%), FBS by (5%), and agarose gel by (7%) with respect to buffered medium can be attributed to the decrease of the exchange rate constant of the amide protons. The k_{ex} in rabbit serum, FBS and agarose gel were found to be 3286 s^{-1}, 3643 s^{-1}, and 3203 s^{-1} respectively. The T_1 relaxivity studies showed significant change in longitudinal relaxation rate constant to water protons in presence of the [Co(**TPTA**)]$^{+2}$ complex. The measured relaxivities were 0.66 mM^{-1} s^{-1} in 20 mM HEPES buffer, 0.28 mM^{-1} s^{-1} in rabbit serum, 0.05 mM^{-1} s^{-1} in FBS and 0.06 mM^{-1} s^{-1} in 4% agarose gel (Fig. S40-S47, ESI†). The T1 relaxivity of [Ni(**TPTA**)Cl]$^{+1}$ complex was found 0.90 mM^{-1} s^{-1} in 20 mM HEPES and 100 mM NaCl. The differences in relaxivity of [Co(**TPTA**)]$^{+2}$ complex do not contribute significantly to the observed differences in CEST peak intensity for different media. It is evident that the CEST intensity of the [Co(**TPTA**)]$^{+2}$ complex in different media mostly depends upon the exchange rate constant of the carboxamide protons. In case of agarose gel the CEST spectra is quite different from other media, as it shows large MT effect between –90 to +90 ppm (Fig. 5). The percentage of CEST effect was calculated by measuring the difference in normalized water peak signal (Mz/M_0%) at +57 ppm and -57 ppm with respect to bulk water.

The CEST effect at pH 7.4 and at 37 ºC was found to be gradually diminishing with decreasing concentration of the complex from 30% at 10 mM to 17% at 3 mM (see Fig. S36, ESI†). However, the complex did not show any appreciable change in CEST effect (negligible dissociation) within the first 24 hours of preparing a solution containing 10 mM [Co(**TPTA**)]$^{+2}$, 100 mM NaCl, 0.4 mM Na_2HPO_4, 25 mM K_2CO_3 at pH 7.80 (Fig. S37, ESI†).

View Article Online
DOI: 10.1039/C9DT00747D

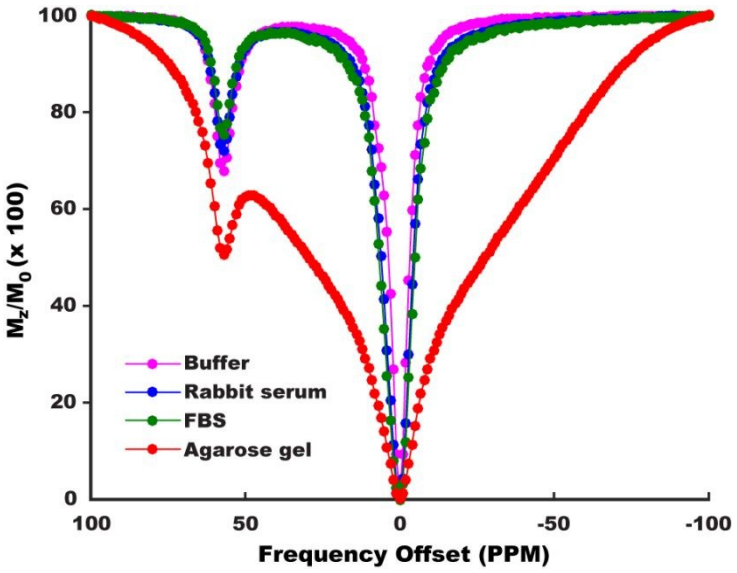

Fig. 6 Overlaid CEST z-spectra of solutions containing 10 mM [Co(**TPTA**)]$^{+2}$ in 20 mM HEPES buffer and 100 mM NaCl at pH 7.4 (magenta), in rabbit serum at pH 7.4 (blue), in FBS at pH 7.4 (green) and in 4% agarose gel, 20 mM HEPES buffer and 100 mM NaCl at pH 7.4 (red).

Table 1. Comparison of Co(II) and Ni(II) complexes of TPTA and similar analogues.

complex	Δω[a]	CEST %	k_{ex} (S^{-1})	T_1 relaxivity ($Mm^{-1}S^{-1}$)
[Co(**TPTA**)]$^{+2}$	57	30[b]	3691[f]	0.66[j]
[Co(**CYNO**)]$^{2+}$	59	38[c]	240 ± 70[g]	0.038[k]
[Co(**TCMC**)]$^{2+}$	45	21.0 ± 0.1[d]	300[h]	0.096[l]
[Co(**CCRM**)]$^{2+}$	112	31.5 ± 0.2[e]	510[i]	0.008[l]
[Ni(**TPTA**)Cl]$^{+1}$	70	5[b]	5096[f]	0.90[j]
[Ni(**CYNO**)]$^{2+}$	72	39 ± 0.2[c]	240 ± 20[g]	0.012[k]
[Ni(**TCMC**)]$^{2+}$	76	12.7 ± 0.9[d]		
[NI(**CCRM**)]$^{2+}$	76	14[e]	328[i]	0.097[l]

[a]The chemical shift of the furthest downfield shifted amide (NH) exchangeable proton versus the water proton resonances. [b]10 mM complex, 100 mM NaCl, and 20 mM of HEPES buffer pH 7.4, B_1= 25 μT, 2 s presaturation radiofrequency pulse at 37 °C, measure on 9.4 T NMR, [c]10 mM complex, 100 mM NaCl, and 20 mM of HEPES buffer pH 7.4, B_1= 24 μT, 2 s presaturation radiofrequency pulse at 37 °C, measure on 11.7 T NMR. [d,e] 10 mM complex, 100 mM NaCl, and 20 mM of HEPES buffer pH 7.4, B_1= 24 μT, 2 s presaturation radiofrequency pulse at 37 °C, measure on 11.7 T NMR. [f]10 mM complex, 100 mM NaCl, and 20 mM of HEPES buffer pH 7.4, at 37 °C, on 9.4 T NMR. [g]8 mM complex, 100 mM NaCl, and 20 mM of HEPES buffer pH 7.4, at 37 °C, on 11.7 T NMR. [h, i]10 mM complex, 100 mM NaCl, and 20 mM of HEPES buffer pH 7.4, at 37 °C, measure on 11.7 T NMR [j] 10 mM complex, 100 mM NaCl, and 20 mM of HEPES buffer pH 7.4, at 37 °C, on 9.4 T NMR. [k]8 mM complex, 100 mM NaCl, and 20 mM of HEPES buffer pH 7.4, at 37 °C, on 11.7 T NMR. [l]10 mM complex, 100 mM NaCl, and 20 mM of HEPES buffer pH 7.4, at 37 °C, on 4.7 T NMR.

It is of interest to compare the CEST spectra of Co(II) and Ni(II) complex of **TPTA** ligand with similar Co(II) and NI (II) macrocyclic ligands in the literature (Table 1). The comparison is made with the furthest shifted CEST peak of Co(II) and Ni (II) complexes of previously reported ligands

View Article Online
DOI: 10.1039/C9DT00747D

7,13-bis(carbamoylmethyl)-1,4,10-trioxa-7,13-diazacyclopentadecane (**CYNO**)[20], 1,4,7,10-tetrakis (carbamoylmethyl)-1,4,7,10-tetraazacyclododecane (**TCMC**)[12, 21] and 1,4,8,11-tetrakis(carbamoylmethyl)-1,4,8,11-tetraazacyclotetradecane (**CCRM**).[12, 21]

Conclusions

We have designed and synthesized a new pyridine containing heptadentate macrocyclic triamide ligand (**TPTA**) for studying the paraCEST properties. [Co(**TPTA**)]$^{+2}$ and [Ni**(TPTA)**Cl]$^{+1}$ complexes have been prepared and their properties have been studied in solution and solid-state. On NMR time scale [Co(**TPTA**)]$^{+2}$ complex produces sharp and highly shifted ^{1}H resonances. Coordination features reveal that Co(II) is seven coordinated with distorted pentagonal bipyramidal geometry and Ni(II) is six coordinated with distorted octahedral geometry. In [Co(**TPTA**)]$^{+2}$ complex all nitrogens of the ring and three amide oxygens from the pendent arms are coordinating to the metal centre whereas in Ni(II) complex two pendent amide arms are not coordinating to the metal centre. The [Co(**TPTA**)]$^{+2}$ complex has shown sharp and intense CEST contrast in buffer, rabbit serum, FBS and agarose gel. The CEST experiment of [Co(**TPTA**)]$^{+2}$ complex in agarose gel shows large MT effect. The [Co(**TPTA**)]$^{+2}$ complex is highly stable in presence of biologically competing anions (high concentration of carbonate and phosphate) and competing metal ion (Zn(II)). The cyclic voltammetry experiment of [Co(**TPTA**)]$^{+2}$ proves that the complex is inert toward oxidation in solution. Most interestingly, the cell viability experiment of [Co(**TPTA**)]$^{+2}$ complex shows that the complex is almost nontoxic up to 10 mM concentration. Overall the [Co(**TPTA**)]$^{+2}$ complex is highly stable in all conditions, nontoxic and gives intense CEST effect in all biological media which suggests that the complex may be useful for in vivo applications.

Experimental Section

Materials and methods

All the reactions were carried out at ambient atmosphere and temperature. $CoCl_2{\cdot}6H_2O$, $NiCl_2{\cdot}6H_2O$, rabbit serum, agarose gel were purchased from Merck. Deuterated solvents were purchased from Sigma-Aldrich. All other chemicals and reagents (analytical and spectroscopic grade) were obtained from commercial sources and used as received. Acetonitrile (MeCN), methanol (MeOH), N,N-Dimethylformamide (DMF), ethanol (EtOH) and diethyl ether (Et_2O) were dried using standard literature methods. pH dependant magnetic measurements of complexes, NMR experiments and dissociation of complexes were carried out by using Expert pro-ISM-IP67 electrode connected to METTLER TOLEDO InLab® 73x series pH meter. pH of CEST experiment was maintained by using Thermo Scientific electrode connected to EUTECH Instruments pH Tutor pH/°C meter. BUCHI M-560 instrument was used to measure the melting points. Elemental analysis was performed using an Elementar vario MICRO cube CHN analyzer. Electro chemical measurements were performed using a CHI 620D electrochemical analyzer equipped with a glassy carbon working electrode, a platinum wire auxiliary electrode, and an Ag/AgCl reference electrode. All the infrared (FT-IR) data were collected with KBr pellets on a BRUKER ALPHA-T FT-IR spectrometer. Perkin-Elmer model Lambda 650 UV-Vis spectrophotometer was used to

View Article Online
DOI: 10.1039/C9DT00747D

record all absorption spectra of ligands and complexes. Evans' measurement, dissociation of complex at different conditions and ^{1}H and ^{13}C NMR spectra were acquired on Bruker AVANCE 400 NMR spectrometer. Bruker microTOF-Q II mass spectrometer was used to collect the mass (ESI-MS) spectra of ligand and complexes.

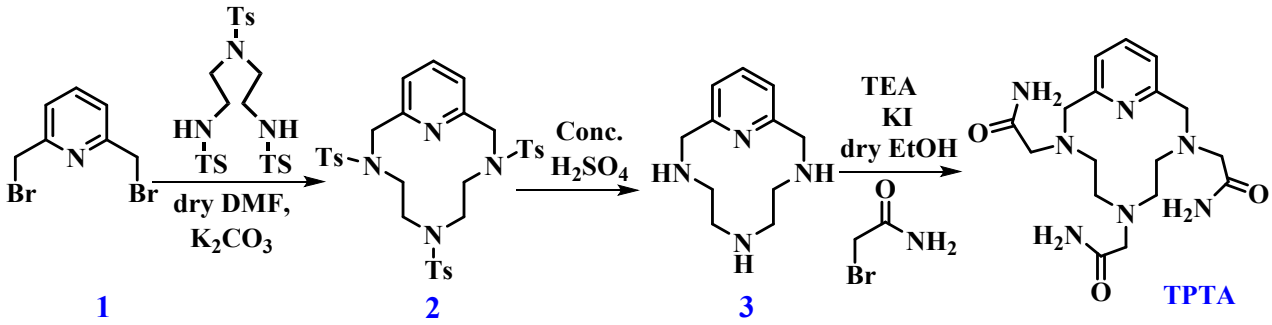

Scheme 1 Synthetic scheme of ligand **TPTA.**

Synthesis of Compound (2). The compound **1** was synthesized by esterification of 2-6-dipicolinic acid and then reduction with sodium borohydride followed by bromination with PBr_3 using the reported literature method.[47] The compound **2** was synthesized by following the reported literature method with slight modification.[39] A mixture of *N*, *N*, *N*''-Tri(toluene-4-sulfonyl)diethylene triamine (3.0 g, 5.30 mmol) and K_2CO_3 (2.2 g, 15.9 mmol) were mixed together in dry DMF (100 mL) and the mixture was stirred and heated to 100 °C under N_2 atmosphere. A solution of 2,6-bis(bromomethyl)pyridine (**1**) (1.4 g, 5.30 mmol) in dry DMF (30 mL) was added dropwise over 30 min. When the addition was completed, the reaction mixture was stirred at 50 °C under N_2 atmosphere for 24 h. After cooling, the reaction mixture was poured into water (75 mL). The resulting precipitate was then filtered and the solid was washed with water and dried in vacuum. The crude product was purified by column chromatography (SiO_2, $CHCl_3$ /EtOAc = 30:1) to give the desired product **2** (2.84 g, 79%) as white powder. mp: 172-174.5 °C. Anal. Calcd for $C_{32}H_{36}N_4O_6S_3$: C, 57.47; H, 5.43; N, 8.38; S, 14.38%. Found: C, 57.83; H, 5.79; N, 7.88; S; 14.17%. ESI-MS m/z: calcd for $C_{32}H_{37}N_4O_6S_3$ ($[MH]^+$), 669.18; found, 669.17; calcd for $C_{32}H_{36}N_4NaO_6S_3$ ($[MNa]^+$), 691.17; found: 691.17. ^{1}H NMR (400 MHz, $CDCl_3$, 25 °C): δ 2.42 (s, 3H), 2.47 (s, 6H), 2.78 (s, 4H), 3.35 (t, J = 7.2 Hz 4H), 4.31 (s, 4H), 7.29 (d, J = 8.4 Hz, 2H), 7.36 (d, J = 8.4 Hz, 4H), 7.45 (d, J = 7.8 Hz, 2H), 7.67 (d, J = 7.8 Hz, 2H), 7.74 (d, J = 8.4 Hz, 4H), 7.78 (d, J = 8.4 Hz, 1H). ^{13}C NMR (100 MHz, $CDCl_3$, 25 °C): δ 155.3 (Ar-CH_2), 143.8 (Ar-SO_2), 143.5 (Ar-SO_2), 139.0 (Ar-H), 136.0 (Ar-CH_3), 135.2 (Ar-CH_3), 130.0 (Ar-H), 129.8 (Ar-H), 127.2 (Ar-H), 127.1 (Ar-H), 124.3 (Ar-H), 55.0 (Ar-CH_2-N), 47.4 (N-CH_2-CH_2-N), 21.6 (Ar-CH_3), 21.5 (Ar-CH_3). FT-IR (KBr, cm^{-1}): 3439 (w, broad); 2925 (w); 1594 (m); 1455 (s); 1358 (s); 1156 (s); 1094 (s); 949 (m); 815 (m); 760 (m); 682 (m); 650 (m); 551 (s).

Synthesis of Compound (3). A mixture of **2** (1 g, 1.29 mmol) and conc. sulfuric acid (10 mL) was stirred at 115-120 °C for 2 h. The reaction mixture was transferred into an erlenmeyer flask having cracked ice, then neutralized by slow addition of 40% NaOH solution until pH reached to 8. The product was extracted with $CHCl_3$ (50 mL) in three portions. The organic phase was dried over $MgSO_4$ and was evaporated to give **3** (0.310g, 80%) as a pale yellow solid. ESI-MS m/z: calcd for $C_{11}H_{19}N_4$ ($[MH]^+$), 207.15; found, 207.16; calcd for $C_{11}H_{18}NaN_4$ ($[MNa]^+$), 229.14; found: 229.14. ^{1}H NMR (400 MHz, $CDCl_3$, 25 °C): δ 2.23 (s, 4H), 2.67 (t, J = 4.8 Hz, 2H), 2.93 (s, 3H), 3.94 (s, 4H), 6.98 (d, J = 8.4 Hz, 2H), 7.50 (t, J = 8.4 Hz, 1H). ^{13}C NMR (100 MHz, $CDCl_3$,

View Article Online
DOI: 10.1039/C9DT00747D

25 °C): δ 159.8 (Ar-CH_2), 136.4 (Ar-H), 119.9 (Ar-H), 53.9 (Ar-CH_2-N), 49.3 (N-CH_2-CH_2-N), 49.0 (N-CH_2-CH_2-N). FT-IR (KBr, cm^{-1}): 3298 (s); 2883 (m); 1577 (s); 1461 (s); 1400 (m); 1345 (m); 1300 (m); 1124 (m); 790 (m).

Synthesis of Ligand (TPTA). The macrocyclic compound **3** (0.240 g, 0.84 mmol), KI (0.153 g, 0.92 mmol) and 2-bromoacetamide (0.463 g, 3.36 mmol) were mixed together in dry ethanol (15 mL) followed by addition of trimethylamine (1 mL, 7.56 mmol). The mixture was heated to 85 °C for 72 h under N_2 atmosphere. Upon completion of reaction, solvent was removed under reduced pressure producing a brown oily residue. The residue was purified by column chromatography on neutral alumina eluting with dichloromethane/methanol (20:1 ratio) to give a light yellow liquid. The light yellow liquid was further purified by dissolving the product in methanol (5 mL) and dropwise addition of diethyl ether to precipitate the product. The precipitate was isolated by filtration, washed with diethyl ether and dried in vacuo to give **TPTA** (0.198g, 52%) as a white powder. mp: 237-239 °C. Anal. Calcd for $C_{17}H_{27}N_7O_3$: C, 54.10; H, 7.21; N, 25.98%. Found: C, 54.83; H, 8.03; N, 26.13%. ESI-MS m/z: calcd for $C_{17}H_{28}N_7O_3$ ($[MH]^+$), 378.22; found, 378.22; calcd for $C_{17}H_{27}N_7NaO_3$ ($[MNa]^+$), 400.21; found: 400.21. ^{1}H NMR (400 MHz, D_2O, ppm): δ = 2.01 (s, 4H), 2.51 (s, 4H), 2.97 (s, 2H), 3.31 (s, 4H), 3.70 (s, 4H), 7.18 (d, J = 7.6 Hz, 2H), 7.68 (t, J = 7.6 Hz, 1H), ^{13}C NMR (100 MHz, D_2O, ppm): 176.2 (C=O), 168.8 (C=O), 158.3 (Ar-CH_2), 138.9 (Ar-H), 121.1 (Ar-H), 60.7 (Ar-CH_2-N), 59.1 (N-CH_2-C=O), 56.0 (N-CH_2-CH_2-N), 52.1 (N-CH_2-C=O), 51.5 (N-CH_2-CH_2-N). UV-vis absorption spectrum (250 μM; 20 mM HEPES, 100 mM NaCl at pH 7.4, 25 °C): 267 nm (ε = 3620 M^{-1} cm^{-1}). FT-IR (KBr, cm^{-1}): 3387 (s); 3299 (s); 3182 (s); 2925 (m); 2843 (m); 1670 (s); 1617 (s); 1384 (s); 1293 (m); 1234 (w); 1163 (w); 1140 (m); 1074 (w); 639 (m).

Synthesis of [Co(TPTA)]·Cl_2·$2H_2O$. A solution of $CoCl_2·6H_2O$ (63 mg, 0.26 mmol) in dry MeOH (5 ml) was added dropwise to a stirring white suspension of **TPTA** (100 mg, 0.26 mmol) in dry MeOH (10 ml) to give a pink colour solution. The reaction mixture was heated gently and was stirred at room temperature for 3 h to get a clear solution. The presence of free Co(II) ion was checked by xylenol orange test. After stirring for 3 h, the solvent was removed and the pink solid was collected and washed with Et_2O and dried under vacuum for 12 h to give pink coloured solid (107mg, 0.21 mmol) of [Co(**TPTA**)]·Cl_2·$2H_2O$. Anal. Calcd for $C_{17}H_{31}Cl_2CoN_7O_5$: C, 37.58; H, 5.75; N, 18.06%. Found: C, 37.51; H, 5.72; N, 17.98%. ESI-MS m/z: calcd for $C_{17}H_{27}N_7O_3Co$ ($[CoL]^{2+}$), 218.07; found, 218.07. UV-vis absorption spectrum (250 μM; 20 mM HEPES, 100 mM NaCl at pH 7.4, 25 °C): 267 nm (ε = 2350 M^{-1} cm^{-1}). FT-IR (KBr, cm^{-1}): 3380 (s); 3292 (s); 3164 (m); 2925 (m); 2908 (m); 1658 (s); 1610 (m); 1453 (m); 1424 (s); 1384 (m); 1234 (w); 1095 (m); 667 (w); 625 (w).

Synthesis of [Ni(TPTA)Cl]·Cl·0.25H_2O. A solution of $NiCl_2·6H_2O$ (63 mg, 0.26 mmol) in dry MeOH (5 ml) was added dropwise to a stirring white suspension of **TPTA** (100 mg, 0.26 mmol) in dry MeOH (10 ml) to give a bluish colour solution. The reaction mixture was heated gently and was stirred at room temperature for 3 h to get a clear solution. The presence of free Ni(II) ion was checked by xylenol orange test. After stirring for 3 h, the solvent was removed and the bluish solid was collected and washed with Et_2O and dried in vacuo for 12 h to give bluish solid (107mg, 0.21 mmol) of [Ni(**TPTA**)Cl]·Cl·0.25H_2O. Anal. Calcd for $C_{17}H27.5Cl_2N_7NiO_{3.25}$: C, 37.53; H, 5.41; N, 19.16%. Found: C, 36.84; H, 5.39; N, 18.58%. ESI-MS m/z: calcd for $C_{17}H_{27}N_7O_3Ni$ ($[NiL]^{2+}$), 217.58; found, 217.57. UV-vis absorption spectrum (250 μM; 20 mM HEPES, 100 mM NaCl at pH 7.4, 25 °C): 264 nm (ε = 3600 M^{-1} cm^{-1}). FT-IR (KBr, cm^{-1}): 3378 (s, broad); 3292 (s); 2927 (w); 1667 (s); 1606 (m); 1462 (m); 1422 (m); 1304 (m); 1093 (m); 668 (w); 634 (w).

View Article Online
DOI: 10.1039/C9DT00747D

Preparation of 4% agarose Gel

The 4% agarose gel solution was prepared by following the same procedure as reported previously.[48] Distilled water (24 ml) was taken in an erlenmeyer flask, then agarose powder (1.0 g) was added portion wise while stirring vigorously at room temperature. The resulting solution was heated to boil until the agarose powder was completely dissolved and the solution became clear. Finally the solution was weighed and appropriate amount of hot distilled water was added to maintain the original mass.

X-ray structure determination

Single crystals of [Co(**TPTA**)]·Cl_2·$2H_2O$ were obtained by vapour diffusion of diethyl ether over the solution of the complex in MeOH and those of nickel [Ni(**TPTA**)Cl]$_2$·Cl_2·$0.5H_2O$ were obtained by slow evaporation of a solution of the complex in a mixture of MeOH and DMF. Suitable single crystals were selected, coated with paraffin oil and mounted on glass fibres. X-ray diffraction data were collected at 110.0 (2) K on a Bruker Kappa APEX III Charge-Coupled Device (CCD) area-detector diffractometer controlled by the APEX3 software package using graphite-monochromated Mo-Kα radiation (λ = 0.71073 Å) and equipped with an Oxford Cryosystems Series 700 cryostream. Diffraction images were processed with the software SAINT-Plus and absorption corrections were applied using program SADABS.[49, 50] The structures were solved by direct methods and refined by full-matrix least squares methods on F^2 using the SHELXTL package.[51] All non-hydrogen atoms were refined anisotropically. Hydrogen atoms were introduced in calculated positions and refined on a riding model with isotropic thermal parameters twenty percent larger than the *U*eq of the attached non-hydrogen atom. Crystal data and the details of structure refinement are provided in Table 2.

Table 2 Crystal data, collection, and structure refinement parameter for [Co(**TPTA**)]·Cl_2·$2H_2O$ and [Ni[**TPTA**)Cl]$_2$·Cl_2·$0.5H_2O$

Parameters	**[Co(TPTA)]·Cl_2·$2H_2O$**	**[Ni(TPTA)Cl]$_2$·Cl_2·$0.5H_2O$**
Empirical formula	C_{17} H_{31} Cl_2 Co N_7 O_5	C_{34} H_{55} Cl_4 N_{14} Ni_2 $O_{6.5}$
Formula weight	543.32	1023.14
Temperature (K)	110(2)	110(2)
Wavelength (Å)	0.71073	0.71073
Crystal system, space gr.	Triclinic, P -1	Triclinic, P -1
a (Å)	9.0833(13)	11.1550(9)
b (Å)	9.9973(15)	14.4670(11)
C (Å)	14.468(2)	16.4988(12)
α (deg)	103.039(7)	65.327(3)
β (deg)	93.097(7)	71.425(3)
γ (deg)	97.532(6)	78.726(3)
Volume (Å^3)	1264.1(3)	2287.4(3)
Z, Calculated density (g/cm^3)	2, 1.427	2, 1.485
Absorption coefficient (mm^{-1})	0.930	1.116
F(000)	566	1066
Crystal size (mm^3)	0.3 x 0.2 x 0.1	0.4 x 0.2 x 0.2
Theta range for data collection	2.265 to 28.696°	2.138 to 28.282°
Limiting indices	-12≤h≤12, -13≤k≤13, -19≤l≤19	-14≤h≤14, -19≤k≤19, -21≤l≤21
Reflections collected / unique	58525 / 6432 [R(int) = 0.1136]	94838 / 11286 [R(int) = 0.0476]

View Article Online
DOI: 10.1039/C9DT00747D

Completeness to theta	99.9 %	99.5%
Absorption correction	Empirical	Empirical
Refinement method	Full-matrix least-squares on F^2	Full-matrix least-squares on F^2
Data / parameters	6432 / 289	11286 / 547
Goodness-of-fit on F^2	1.163	1.040
Final R indices [I>2σ (I)]	R1 = 0.1013, wR2 = 0.3153	R1 = 0.0526, wR2 = 0.1702
R indices (all data)	R1 = 0.1463, wR2 = 0.3545	R1 = 0.0638, wR2 = 0.1815
Largest diff. peak and hole (e.$Å^{-3}$)	1.511 and -1.075	1.874 and -0.799

$$R1 = \sum[|F_o| - |F_c|]/\sum|F_o|, wR2 = [\sum[w(|F_o|^2 - |F_c|^2)^2]/\sum[w(|F_o|^2)^2]]^{1/2}$$

Determination of solution magnetic moment

Evans method [52, 53] was used to calculate the effective magnetic moments of complexes**.** In order to determine the magnetic moments of the complexes at different pH, (3-6 mM) of complex was dissolved in a buffer solution containing 20 mM HEPES, 100 mM NaCl, 5% (v/v) tert-butanol and 10% (v/v) D_2O. The pH of all solutions were maintained to the exact value by addition of 0.5 N HCl and NaOH respectively. The resulting solution was placed in a sealed capillary tube inside the NMR tube containing same solvent without paramagnetic complex, as a reference solution. Magnetic susceptibility of complexes at variable pH were calculated by ^{1}H NMR spectra on a Bruker AVANCE III 400 MHz spectrometer at 310 K (T). Diamagnetic corrections were carried based on the empirical formula using Pascal's constant.[54] The effective magnetic moments (μ_{eff}) was calculated using the following equation (1):

$$\chi_g = \frac{-3\Delta\nu}{4\pi\nu_0} + \chi_0 + \frac{[\chi_0(d_0 - d_s]}{m} \qquad (1)$$

In this equation Δν is the difference of frequency (Hz) observed for tert-butanol in the sample and the reference solutions. ν_0 is the spectrometer frequency (Hz), m is the mass of the substance per cm^3 of solution and χ_0 is the mass susceptibility of solvent H_2O (-0.72 x 10^{-6} cm^3/g for the dilute aqueous *tert*-butanol). The last term is neglected here due to minimal contribution of mass susceptibility.

Dissociation of complex

^{1}H NMR spectroscopy was used to monitor the stability of complexes under acidic condition, in presence of biologically relevant ions and other competing transition metal cations. To assess the stability of $[Co(\mathbf{TPTA})]^{+2}$ in acidic condition, sample contained 10 mM complex, 100 mM NaCl, (3-5) mM 3-(trimethylsilyl)-1-propanesulfonic acid sodium salt as a standard at pD 3.6-4.3. For studies in the presence of biologically relevant ions, sample contained 10 mM complex, 100 mM NaCl, 25 mM K_2CO_3, 0.40 mM Na_2HPO_4 and 5 mM of 3-(trimethylsilyl)-1-propanesulfonic acid sodium salt as a standard at pD 7.4-8.0. For studies with other metal cation, sample contained 10 mM $ZnCl_2$, 100 mM NaCl, 5 mM of 3-(trimethylsilyl)-1-propanesulfonic acid sodium salt as a standard at pD 6.8-7.1. All the samples were kept in an incubator at 37 °C and monitored for 72 h. The pD of all solution were maintained to the exact value by addition of dilute DCl and/or NaOD.

View Article Online
DOI: 10.1039/C9DT00747D

Electrochemical measurement

Cyclic voltammetric measurement was carried out by using CHI 620D electrochemical analyzer at ambient temperature under nitrogen atmosphere. The cell was equipped with a glassy carbon working electrode, a platinum wire as a counter electrode, and an Ag/AgCl as a reference electrode. The measurement was carried out in aqueous solution with 1 mM complex, 20 mM HEPES, 100 mM NaCl at pH 7.4 with a scan rate 100 mV s^{-1}. The observed potentials with respect to Ag/AgCl electrode were converted and referenced to the normal hydrogen electrode (NHE) by using standard reported literature conversion factor.[55]

NMR spectroscopy

^{1}H and ^{13}C NMR spectra of Ligand and its intermediates were recorded at 25 ºC at 400 MHz and 100 MHz frequencies, respectively using Bruker AVANCE III 400 MHz spectrometer. Variable-temperature ^{1}H NMR spectra and ^{1}H-^{1}H-COSY spectrum of complexes were recorded on the same spectrometer. ^{1}H NMR spectra of 10 mM solution of complexes at various pH were recorded at 37 ºC in presence of 20 mM HEPES and 100 mM NaCl. The pH of all the solutions were maintained at the preferred value by addition of 0.5 N HCl and NaOH. For analysis and processing of the recorded spectra, Topspin 3.5pl7 and MestReNova 10.0 NMR data processing software were used. Lock was achieved by placing one sealed glass capillary containing D_2O inside the 5 mm NMR tube.

CEST experiment

CEST experiments were performed on a 9.4 Tesla 400 MHz Bruker AVANCE-III Nanobay NMR spectrometer using a broadband liquid state probe-head. CEST z-spectra were obtained by plotting normalized (100 x M_z/M_0) water signal intensities as a function of the presaturation pulse frequency offset from the bulk water. Spectra were collected with presaturation at 1 ppm interval with respect to the bulk water resonance position. Presaturation was achieved at a power level of 25 μT with duration of 2 s pulse. Spectra of 10 mM complexes were collected at 37 ºC in the presence of 20 mM HEPES and 100 mM NaCl. To monitor the efficiency of the complex as a CEST agent in biological media, separate 10 mM solutions of the complexes were prepared in rabbit serum, fetal bovine serum (FBS) and agarose gel. All spectra were recorded at 37 °C. To determine the CEST spectra in agarose gel, solution was prepared by diluting 1 ml of 20 mM complex, 40 mM HEPES and 200 mM NaCl in 1 ml of 4 % agarose gel solution and finally adjusting the pH to 7.4. The pH values of the buffer solution, rabbit serum, fetal bovine serium (FBS) and agarose gel samples were adjusted using 0.5 N HCl and NaOH solution. Lock was achieved by placing one sealed glass capillary containing D_2O inside the 5 mm NMR tube.

Determination of Exchange Rate Constant

NMR Exchange rate constant of [Co(**TPTA**)]$^{+2}$ complex in the four media listed above was determined by measuring the water signal intensities immediately after on-resonance (M_z) and off-resonance (M_0) irradiation of 4 s to ensure the complete saturation at different pre-saturation power

View Article Online
DOI: 10.1039/C9DT00747D

levels (B_1) ranging between 7.5 μT to 25 μT. The calculation of exchange constant (k_{ex}) was performed following the procedure described by Dixon *et. al.*[56] The expected linear relationship between the quantity $M_z/(M_0 - M_z)$ and $1/\omega_1^2$ was fitted in Microsoft Excel with high correlation coefficient of 0.998. ω_1 is given by γB_1, γ being the gyro-magnetic ratio of proton. The exchange constant was then calculated from the intercept on the $1/\omega_1^2$ axis as $1/k_{ex}^2 = -1/\omega_1^2$

T_1 relaxivity

Longitudinal relaxation rate constant for water protons both in absence and presence of [Co(**TPTA**)]$^{+2}$ complex was measured using the inversion recovery method. Relaxation of inverted bulk water magnetization was monitored as a function of 8 decay intervals ranging from 6 ms to 10 s. Long repetition time (recycle delay) of 5 s was employed to ensure complete longitudinal relaxation between two measurements. The relaxivity was calculated as the concentration normalized change in longitudinal rate constant of water in presence of the complex from that of free water (in absence of the complex).

Cell culture and cytotoxicity

HEK 293 WT were maintained in culture flasks in DMEM supplemented with 10% heat-inactivated FBS (Gibco), antibiotic cocktail (1 mM penicillin, 1 mM streptomycin) and 2 mM L-glutamine. Cells were cultured and maintained in a humidified atmosphere at 37°C and 5% CO_2. Cytotoxicity was measured by the MTT (3-(4,5-Dimethyl-2-thiazolyl)-2,5-diphenyl-2H-tetrazolium bromide) method as described earlier.[57] Cells (100 μl) were seeded (concentration 5-7 × 10^5 cells/mL) into a microtitre plate and incubated for 24 h to allow them to adhere.

[Co(**TPTA**)]$^{+2}$ complex was dissolved in double distilled water to a stock solution of 200 mM. Further, working dilutions were made tn the concentration range of 20 to 200 mM and 20μl of diluted compound was added to 400μl media such that the final concentration would range from 1 mM to 10 mM respectively. The negative control wells included cells exposed to 20 μl ddH_2O. Post compound addition, the microtitre plate was incubated for additional 24 h and the cytotoxitiy was assayed using the thiazolyl blue tetrazolium bromide (MTT) colorimetric assay. The assay is based on the ability of live cells to reduce the water soluble MTT into an insoluble formazan product. Briefly, after a 24 h incubation, 10μl of MTT (5 mg/ml) was added to the cells and incubated for 5 h. Absorbance of the developed colour was spectrophotometrically determined using a multi-well plate reader which measured the optical density at 570 nm with a reference wavelength of 655 nm. Data expressed as mean ± standard error (SE) for each experimental group were analyzed by one way analysis of variance (ANOVA) using GraphPad Prism statistical software package version 7.0 (San Diego, USA).

Conflicts of interest

The authors declare no conflict of interest.

View Article Online
DOI: 10.1039/C9DT00747D

Acknowledgements

AKS acknowledges IIT Bhubaneswar for infrastructure. RNP thanks UGC, Delhi for his fellowship. AG acknowledges NISER (DAE) for infrastructure. SC acknowledges NISER for the fellowship. PB thanks UGC, Delhi for Junior and Senior research fellowship.

Notes and references

1. V. C. Pierre, M. J. Allen and P. Caravan, *Journal of biological inorganic chemistry : JBIC : a publication of the Society of Biological Inorg. Chem.*, 2014, **19**, 127-131.
2. D. W. McRobbie, E. A. Moore, M. J. Graves and M. R. Prince, MRI from Picture to Proton, Cambridge University Press, Cambridge, 2 edn., 2006.
3. P. Caravan, *Chem. Soc. Rev.*, 2006, **35**, 512-523.
4. R. B. Lauffer, *Chem. Rev.*, 1987, **87**, 901-927.
5. K. N. Raymond and V. C. Pierre, *Bioconjugate Chem.*, 2005, **16**, 3-8.
6. P. Caravan, J. J. Ellison, T. J. McMurry and R. B. Lauffer, *Chem. Rev.*, 1999, **99**, 2293-2352.
7. N. Richardson, J. A. Davies and B. Radüchel, *Polyhedron*, 1999, **18**, 2457-2482.
8. R. Pollet, C. S. Bonnet, P. Retailleau, P. Durand and É. Tóth, *Inorg. Chem.*, 2017, **56**, 4317-4323.
9. E. Terreno, D. D. Castelli, A. Viale and S. Aime, *Chem. Rev.*, 2010, **110**, 3019-3042.
10. i A. S. Merbach, L. Helm and É. Tóth, *The Chemistry of Contrast Agents in Medical Magnetic Resonance Imaging,* 2nd ed. Wiley, ISBN: 9781119991762, 2013
11. M. Woods, D. E. Woessner and A. D. Sherry, *Chem. Soc. Rev.*, 2006, **35**, 500-511.
12. S. J. Dorazio, A. O. Olatunde, P. B. Tsitovich and J. R. Morrow, *JBIC Journal of Biological Inorganic Chemistry*, 2014, **19**, 191-205.
13. S. Zhang, C. R. Malloy and A. D. Sherry, *J. Am. Chem. Soc.*, 2005, **127**, 17572-17573.
14. M. Milne, M. Lewis, N. McVicar, M. Suchy, R. Bartha and R. H. E. Hudson, *RSC Advances*, 2014, **4**, 1666-1674.
15. S. J. Ratnakar, T. C. Soesbe, L. L. Lumata, Q. N. Do, S. Viswanathan, C.-Y. Lin, A. D. Sherry and Z. Kovacs, *J. Am. Chem. Soc.*, 2013, **135**, 14904-14907.
16. D. L. Longo, A. Bartoli, L. Consolino, P. Bardini, F. Arena, M. Schwaiger and S. Aime, *Cancer Research*, 2016, **76**, 6463.
17. N. Cakić, B. Tickner, M. Zaiss, D. Esteban-Gómez, C. Platas-Iglesias and G. Angelovski, *Inorg. Chem.*, 2017, **56**, 7737-7745.
18. P. J. Burns, J. M. Cox and J. R. Morrow, *Inorg. Chem.*, 2017, **56**, 4545-4554.
19. S. J. Dorazio and J. R. Morrow, *Inorg. Chem.*, 2012, **51**, 7448-7450.
20. A. O. Olatunde, J. M. Cox, M. D. Daddario, J. A. Spernyak, J. B. Benedict and J. R. Morrow, *Inorg. Chem.*, 2014, **53**, 8311-8321.
21. A. O. Olatunde, C. J. Bond, S. J. Dorazio, J. M. Cox, J. B. Benedict, M. D. Daddario, J. A. Spernyak and J. R. Morrow, *Chemistry – A Eur. J.*, 2015, **21**, 18290-18300.
22. A. O. Olatunde, S. J. Dorazio, J. A. Spernyak and J. R. Morrow, *J. Am. Chem. Soc.*, 2012, **134**, 18503-18505.
23. A. E. Thorarinsdottir, K. Du, J. H. P. Collins and T. D. Harris, *J. Am. Chem. Soc.*, 2017, **139**, 15836-15847.

View Article Online
DOI: 10.1039/C9DT00747D

24. S. J. Dorazio, P. B. Tsitovich, K. E. Siters, J. A. Spernyak and J. R. Morrow, *J. Am. Chem. Soc.*, 2011, **133**, 14154-14156.
25. Lvano Bertini and C. Luchinat, *San Francisco, CA*, 1986.
26. I. Bertini, C. Luchinat, G. Parigi and R. Pierattelli, *ChemBioChem*, 2005, **6**, 1536-1549.
27. I. Bertini, P. Turano and A. J. Vila, *Chem. Rev.*, 1993, **93**, 2833-2932.
28. K. M. Ward, A. H. Aletras and R. S. Balaban, *J. Mag. Reson.*, 2000, **143**, 79-87.
29. W. Ling, R. R. Regatte, G. Navon and A. Jerschow, *Proceedings of the National Academy of Sciences*, 2008, **105**, 2266.
30. M. T. McMahon, A. A. Gilad, J. Zhou, P. Z. Sun, J. W. M. Bulte and P. C. M. van Zijl, *Mag. Reson. Med.*, 2006, **55**, 836-847.
31. S. J. Ratnakar, S. Viswanathan, Z. Kovacs, A. K. Jindal, K. N. Green and A. D. Sherry, *J. Am. Chem. Soc.*, 2012, **134**, 5798-5800.
32. R.-A. F. Rarig, M. N. Tran and D. M. Chenoweth, *J. Am. Chem. Soc.*, 2013, **135**, 9213-9219.
33. D. L. Longo, F. Z. Moustaghfir, A. Zerbo, L. Consolino, A. Anemone, M. Bracesco and S. Aime, *Int. J. Pharm.*, 2017, **525**, 275-281.
34. E. Vinogradov, A. D. Sherry and R. E. Lenkinski, *J. Mag. Reson.*, 2013, **229**, 155-172.
35. S. Viswanathan, Z. Kovacs, K. N. Green, S. J. Ratnakar and A. D. Sherry, *Chem. Rev.*, 2010, **110**, 2960-3018.
36. S. J. Dorazio, A. O. Olatunde, J. A. Spernyak and J. R. Morrow, *Chem. Commun.*, 2013, **49**, 10025-10027.
37. K. Srivastava, G. Ferrauto, V. G. Young, S. Aime and V. C. Pierre, *Inorg. Chem.*, 2017, **56**, 12206-12213.
38. A. E. Thorarinsdottir, S. M. Tatro and T. D. Harris, *Inorg. Chem.*, 2018, **57**, 11252-11263.
39. J. Serrano-Plana, A. Aguinaco, R. Belda, E. García-España, M. G. Basallote, A. Company and M. Costas, *Angew. Chem. Int. Ed.*, 2016, **55**, 6310-6314.
40. I. Ali, W. A. Wani and K. Saleem, *Synthesis and Reactivity in Inorganic, Metal-Organic, and Nano-Metal Chemistry*, 2013, **43**, 1162-1170.
41. P. B. Tsitovich, J. M. Cox, J. B. Benedict and J. R. Morrow, *Inorg. Chem.*, 2016, **55**, 700-716.
42. L. Sacconi, F. Mani and A. Bencini, *Eds. Pergamon Press: Oxford, UK*, 1987, **5**.
43. P. M. Wood, *Biochem. J*, 1988, **253**, 287-289.
44. S. Aime, D. Delli Castelli and E. Terreno, *Angew. Chem. Int. Ed.*, 2002, **41**, 4334-4336.
45. P. B. Tsitovich and J. R. Morrow, *Inorg. Chim. Acta*, 2012, **393**, 3-11.
46. S. Aime, A. Barge, D. Delli Castelli, F. Fedeli, A. Mortillaro, F. U. Nielsen and E. Terreno, *Mag. Reson. Med.*, 2002, **47**, 639-648.
47. W. Chen, X. Tang, W. Dou, Z. Ju, B. Xu, W. Xu and W. Liu, *Chem. Commun.*, 2016, **52**, 5124-5127.
48. F. M. Buck, W. C. Bae, E. Diaz, J. Du, S. Statum, E. T. Han and C. B. Chung, *Am. J. Roent.* 2011, **196**, W174-W179.
49. *APEX2 and SAINT, Bruker AXS Inc., Madison, WI*, 2016.
50. G. M. Sheldrick, *Acta crystallographica. Section A, Foundations of crystallography*, 2008, **64**, 112-122.
51. G. M. Sheldrick, SHELXS97 and SHELXL97. Program for Crystal Structure Solution and Refinement. University of Göttingen, Göttingen. 1997
52. D. F. Evans, *J. Chem. Soc.*, 1959, 2003-2005.

View Article Online
DOI: 10.1039/C9DT00747D

53. E. M. Schubert, *J. Chem. Educ.*, 1992, **69**, 62.
54. G. A. Bain and J. F. Berry, *J. Chem. Educ.*, 2008, **85**, 532.
55. G. D. Christian, *Analytical chemistry*, 4th ed. Wiley: New York 1986, 290.
56. W. T. Dixon, J. Ren, A. J. M. Lubag, J. Ratnakar, E. Vinogradov, I. Hancu, R. E. Lenkinski and A. D. Sherry, *Mag. Reson. Med.*, 2010, **63**, 625-632.
57. M. V. Berridge and A. S. Tan, *Arch. Biochem. Biophys.*, 1993, **303**, 474-482.

For Table of Contents Entry

View Article Online
DOI: 10.1039/C9DT00747D

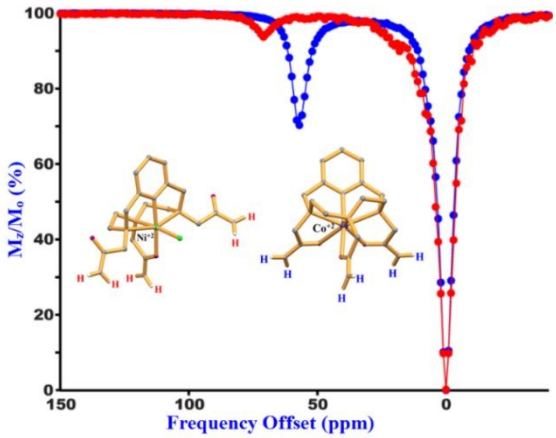

Co(II) and Ni(II) complexes of a macrocyclic triamide ligand act as paraCEST MRI contrast agent in HEPES buffer, FBS, rabbit serum and 4% agarose gel (w/w).